

# Cascaded Current–Voltage Control to Improve the Power Quality for a Grid-Connected Inverter With a Local Load

Qing-Chang Zhong, *Senior Member, IEEE*, and Tomas Hornik, *Member, IEEE*

**Abstract**—In this paper, a cascaded current–voltage control strategy is proposed for inverters to simultaneously improve the power quality of the inverter local load voltage and the current exchanged with the grid. It also enables seamless transfer of the operation mode from stand-alone to grid-connected or *vice versa*. The control scheme includes an inner voltage loop and an outer current loop, with both controllers designed using the  $H^\infty$  repetitive control strategy. This leads to a very low total harmonic distortion in both the inverter local load voltage and the current exchanged with the grid at the same time. The proposed control strategy can be used to single-phase inverters and three-phase four-wire inverters. It enables grid-connected inverters to inject balanced clean currents to the grid even when the local loads (if any) are unbalanced and/or nonlinear. Experiments under different scenarios, with comparisons made to the current repetitive controller replaced with a current proportional–resonant controller, are presented to demonstrate the excellent performance of the proposed strategy.

**Index Terms**— $H^\infty$  control, microgrids, power quality, repetitive control, seamless transfer, total harmonic distortion (THD).

## I. INTRODUCTION

MICROGRIDS are emerging as a consequence of rapidly growing distributed power generation systems. Improving the control capabilities and operational features of microgrids brings environmental and economic benefits. The introduction of microgrids leads to improved power quality, reduces transmission congestion, decreases emission and energy losses, and effectively facilitates the utilization of renewable energy. Microgrids are normally operated in the grid-connected mode; however, it is also expected to provide sufficient generation capacity, controls, and operational strategies to supply at least a part of the load after being disconnected from the distribution system and to remain operational as a stand-

alone (islanded) system [1]–[6]. Traditionally, the inverters used in microgrids behave as current sources when they are connected to the grid and as voltage sources when they work autonomously [7]. This involves the change of the controller when the operational mode is changed from stand-alone to grid-connected or *vice versa* [8]. It is advantageous to operate inverters as voltage sources because there is no need to change the controller when the operation mode is changed. A parallel control structure consisting of an output voltage controller and a grid current controller was proposed in [8] to achieve seamless transfer via changing the references to the controller without changing the controller. Another important aspect for grid-connected inverters or microgrids is the active and reactive power control; see, e.g., [9] and [10] for more details.

As nonlinear and/or unbalanced loads can represent a high proportion of the total load in small-scale systems, the problem with power quality is a particular concern in microgrids [11]. Moreover, unbalanced utility grid voltages and utility voltage sags, which are two most common utility voltage quality problems, can affect microgrid power quality [12], [13]. The inverter controller should be able to cope with unbalanced utility grid voltages and voltage sags, which are within the range given by the waveform quality requirements of the local loads and/or microgrids. When critical loads are connected to an inverter, severe unbalanced voltages are not generally acceptable, and the inverter should be disconnected from the utility grid. Only when the voltage imbalance is not so serious or the local load is not very sensitive to it can the inverter remain connected. Since the controllers designed in the  $dq$  or  $\alpha\beta$  frames under unbalanced situations become noticeably complex [14], it is advantageous to design the controller in the natural reference frame.

Another power quality problem in microgrids is the total harmonic distortion (THD) of the inverter local load voltage and the current exchanged with the grid (referred to as the grid current in this paper), which needs to be maintained low according to industrial regulations. It has been known that it is not a problem to obtain low THD either for the inverter local load voltage [15], [16] or for the grid current [17], [18]. However, no strategy has been reported in the literature to obtain low THD for both the inverter local load voltage and the grid current simultaneously. This may even have been believed impossible because there may be nonlinear local loads. In this paper, a cascaded control structure consisting of an inner-loop voltage controller and an outer-loop current controller is proposed to achieve this, after spotting that the inverter  $LCL$  filter can be split into two separate parts (which

Manuscript received February 28, 2011; revised May 16, 2011 and September 29, 2011; accepted January 9, 2012. Date of publication February 10, 2012; date of current version November 22, 2012. The work of Q.-C. Zhong was supported in part by the Engineering and Physical Sciences Research Council (EPSRC), U.K., under Grant EP/J001333/1. The work of T. Hornik was supported by the EPSRC, U.K., under the doctoral training account scheme. An earlier version of this paper was presented at the 36th Annual Conference of the IEEE Industrial Electronics Society, Glendale, AZ, November 2010.

Q.-C. Zhong is with the Department of Automatic Control and Systems Engineering, The University of Sheffield, S1 3JD Sheffield, U.K. (e-mail: Q.Zhong@Sheffield.ac.uk).

T. Hornik was with the Department of Electrical Engineering and Electronics, The University of Liverpool, L69 3GJ Liverpool, U.K. He is now with Turbo Power Systems, UB7 OLJ West Drayton, U.K.

Color versions of one or more of the figures in this paper are available online at <http://ieeexplore.ieee.org>.

Digital Object Identifier 10.1109/TIE.2012.2187415

is, of course, obvious but nobody has taken advantage of it). The  $LC$  part can be used to design the voltage controller, and the grid interface inductor can be used to design the current controller. The voltage controller is responsible for the power quality of the inverter local load voltage and power distribution and synchronization with the grid, and the current controller is responsible for the power quality of the grid current, the power exchanged with the grid, and the overcurrent protection. With the help of the  $H^\infty$  repetitive control [16]–[18], the proposed strategy is able to maintain low THD in both the inverter local load voltage and the grid current at the same time. When the inverter is connected to the grid, both controllers are active; when the inverter is not connected to the grid, the current controller is working under zero current reference. Hence, no extra effort is needed when changing the operation mode of the inverter, which considerably facilitates the seamless mode transfer for grid-connected inverters. For three-phase inverters, the same individual controller can be used for each phase in the natural frame when the system is implemented with a neutral-point controller, e.g., the one proposed in [19]. As a result, the inverter can cope with unbalanced local loads for three-phase applications. In other words, harmonic currents and unbalanced local load currents are all contained locally and do not affect the grid. Experimental results are presented to demonstrate the excellent performance of the proposed control scheme.

It is worth stressing that the cascaded current–voltage control structure improves the quality of both the inverter local load voltage and the grid current at the same time and achieves seamless transfer of the operation mode. The outer-loop current controller provides a reference for the inner-loop voltage controller, which is the key to allow the simultaneous improvement of the THD in the grid current and the inverter local load voltage and to achieve the seamless transfer of operation mode. This is different from the conventional voltage–current control scheme [12], where the (inner) current loop is used to regulate the filter inductor current of the inverter (not the grid current), so it is impossible to achieve simultaneous improvement of the THD in the grid current and the inverter local load voltage. An inner current loop can still be added to the proposed structure inside the voltage loop without any difficulty to perform the conventional function, if needed. The  $H^\infty$  repetitive control strategy [16]–[18] is adopted in the paper to design the controllers, but this is not a must; other approaches can be used as well. Repetitive control [20], which is regarded as a simple learning control method, provides an alternative to perfectly track periodic signals and/or to reject periodic disturbances in dynamic systems, using the internal model principle [21]. The internal model is infinite dimensional and can be obtained by connecting a delay line into a feedback loop. Such a closed-loop system can deal with a very large number of harmonics simultaneously, as it has high gains at the fundamental and all harmonic frequencies of interest. It has been successfully applied to constant-voltage constant-frequency pulse-width modulated (PWM) inverters [22]–[26], grid-connected inverters [15], [27], and active filters [28], [29] to obtain very low THD. The multiloop control strategies analyzed in [30] indicated that it was impossible to stabilize an inverter with a proportional feedback of the capacitor voltage and that the performance with an inner-

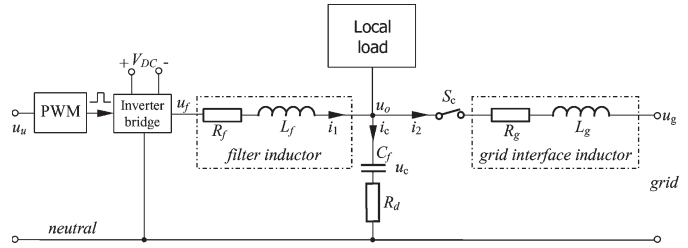


Fig. 1. Sketch of a grid-connected single-phase inverter with local loads.

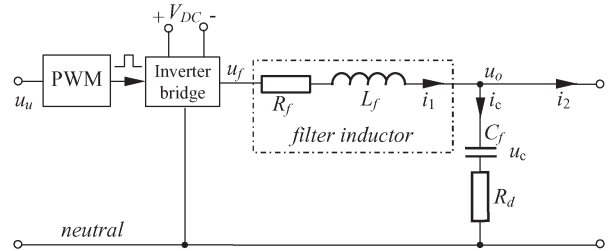


Fig. 2. Control plant  $P_u$  for the inner voltage controller.

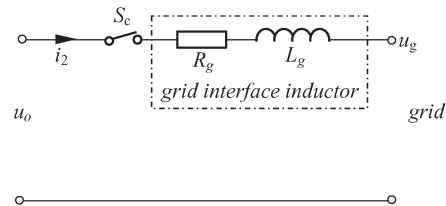


Fig. 3. Control plant  $P_i$  for the outer current controller.

loop proportional–derivative voltage controller was not good either. This paper has demonstrated that excellent performance can be achieved with an inner-loop repetitive controller.

The rest of this paper is organized as follows. The proposed control scheme is presented in Section II, followed by the voltage controller designed in Section III and the current controller designed in Section IV. An example design is described in Section V, and extensive experimental results are presented and discussed in Section VI. Finally, conclusions are made in Section VII.

## II. PROPOSED CONTROL SCHEME

Fig. 1 shows the structure of a single-phase inverter connected to the grid. It consists of an inverter bridge, an  $LC$  filter, and a grid interface inductor connected with a circuit breaker. It is worth noting that the local loads are connected in parallel with the filter capacitor. The current  $i_1$  flowing through the filter inductor is called the filter inductor current in this paper, and the current  $i_2$  flowing through the grid interface inductor is called the grid current in this paper. The control objective is to maintain low THD for the inverter local load voltage  $u_o$  and, simultaneously, for the grid current  $i_2$ . As a matter of fact, the system can be regarded as two parts, as shown in Figs. 2 and 3, cascaded together. Hence, a cascaded controller can be adopted and designed. The proposed controller, as shown in Fig. 4, consists of two loops: an inner voltage loop to regulate the inverter local load voltage  $u_o$  and an outer current loop to

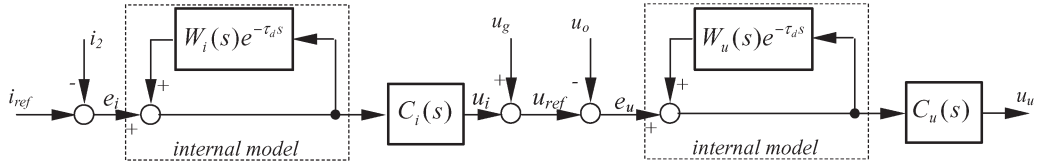


Fig. 4. Proposed cascaded current–voltage controller for inverters, where both controllers adopt the  $H^\infty$  repetitive strategy.

regulate the grid current  $i_2$ . According to the basic principles of control theory about cascaded control, if the dynamics of the outer loop is designed to be slower than that of the inner loop, then the two loops can be designed separately. As a result, the outer-loop controller can be designed under the assumption that the inner loop is already in the steady state, i.e.,  $u_o = u_{\text{ref}}$ . It is also worth stressing that the current controller is in the outer loop and the voltage controller is in the inner loop. This is contrary to what is normally done. In this paper, both controllers are designed using the  $H^\infty$  repetitive control strategy because of its excellent performance in reducing THD.

The main functions of the voltage controller are the following: to deal with power quality issues of the inverter local load voltage even under unbalanced and/or nonlinear local loads, to generate and dispatch power to the local load, and to synchronize the inverter with the grid. When the inverter is synchronized and connected with the grid, the voltage and the frequency are determined by the grid.

The main function of the outer-loop current controller is to exchange a clean current with the grid even in the presence of grid voltage distortion and/or nonlinear (and/or unbalanced for three-phase applications) local loads connected to the inverter. The current controller can be used for overcurrent protection, but normally, it is included in the drive circuits of the inverter bridge. A phase-locked loop (PLL) can be used to provide the phase information of the grid voltage, which is needed to generate the current reference  $i_{\text{ref}}$  (see Section V for an example). As the control structure described here uses just one inverter connected to the system and the inverter is assumed to be powered by a constant dc voltage source, no controller is needed to regulate the dc-link voltage (otherwise, a controller can be introduced to regulate the dc-link voltage).

Another important feature is that the grid voltage  $u_g$  is fed forward and added to the output of the current controller. This is used as a synchronization mechanism, and it does not affect the design of the controller, as will be seen later.

### III. DESIGN OF THE VOLTAGE CONTROLLER

The design of the voltage controller will be outlined hereinafter, following the detailed procedures proposed in [16]. A prominent feature different from what is known is that the control plant of the voltage controller is no longer the whole  $LCL$  filter but just the  $LC$  filter, as shown in Fig. 2.

#### A. State-Space Model of the Plant $P_u$

The corresponding control plant shown in Fig. 2 for the voltage controller consists of the inverter bridge and the  $LC$  filter ( $L_f$  and  $C_f$ ). The filter inductor is modeled with a series

winding resistance. The PWM block, together with the inverter, is modeled by using an average voltage approach with the limits of the available dc-link voltage [15] so that the average value of  $u_f$  over a sampling period is equal to  $u_u$ . As a result, the PWM block and the inverter bridge can be ignored when designing the controller.

The filter inductor current  $i_1$  and the capacitor voltage  $u_c$  are chosen as state variables  $x_u = [i_1 \ u_c]^T$ . The external input  $w_u = [i_2 \ u_{\text{ref}}]^T$  consists of the grid current  $i_2$  and the reference voltage  $u_{\text{ref}}$ . The control input is  $u_u$ . The output signal from the plant  $P_u$  is the tracking error  $e_u = u_{\text{ref}} - u_o$ , where  $u_o = u_c + R_d(i_1 - i_2)$  is the inverter local load voltage. The plant  $P_u$  can be described by the state equation

$$\dot{x}_u = A_u x_u + B_{u1} w_u + B_{u2} u_u \quad (1)$$

and the output equation

$$y_u = e_u = C_{u1} x_u + D_{u1} w_u + D_{u2} u_u \quad (2)$$

with

$$A_u = \begin{bmatrix} -\frac{R_f + R_d}{L_f} & -\frac{1}{L_f} \\ \frac{1}{C_f} & 0 \end{bmatrix}$$

$$B_{u1} = \begin{bmatrix} \frac{R_d}{L_f} & 0 \\ -\frac{1}{C_f} & 0 \end{bmatrix} \quad B_{u2} = \begin{bmatrix} \frac{1}{L_f} \\ 0 \end{bmatrix}$$

$$C_{u1} = [-R_d \quad -1]$$

$$D_{u1} = [R_d \quad 1] \quad D_{u2} = 0.$$

The corresponding plant transfer function is then

$$P_u = \left[ \begin{array}{c|cc} A_u & B_{u1} & B_{u2} \\ \hline C_{u1} & D_{u1} & D_{u2} \end{array} \right]. \quad (3)$$

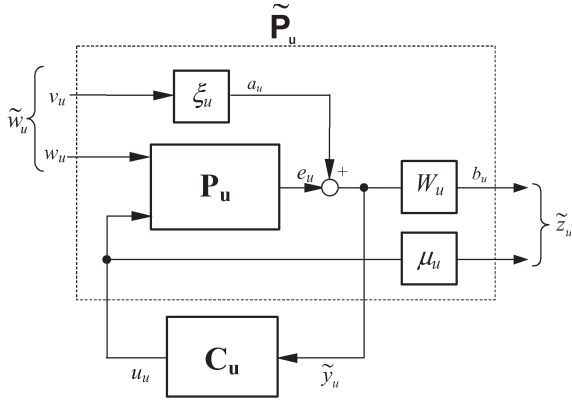
#### B. Formulation of the Standard $H^\infty$ Problem

In order to guarantee the stability of the inner voltage loop, an  $H^\infty$  control problem, as shown in Fig. 5, is formulated to minimize the  $H^\infty$  norm of the transfer function  $T_{\tilde{z}_u \tilde{w}_u} = \mathcal{F}_l(\tilde{P}_u, C_u)$  from  $\tilde{w}_u = [v_u \ w_u]^T$  to  $\tilde{z}_u = [z_{u1} \ z_{u2}]^T$ , after opening the local positive feedback loop of the internal model and introducing weighting parameters  $\xi_u$  and  $\mu_u$ . The closed-loop system can be represented as

$$\begin{bmatrix} \tilde{z}_u \\ \tilde{y}_u \end{bmatrix} = \tilde{P}_u \begin{bmatrix} \tilde{w}_u \\ u_u \end{bmatrix}$$

$$u_u = C_u \tilde{y}_u \quad (4)$$

where  $\tilde{P}_u$  is the generalized plant and  $C_u$  is the voltage controller to be designed. The generalized plant  $\tilde{P}_u$  consists of


 Fig. 5. Formulation of the  $H^\infty$  control problem for the voltage controller.

the original plant  $P_u$ , together with the low-pass filter  $W_u = \begin{bmatrix} A_{w_u} & B_{w_u} \\ C_{w_u} & D_{w_u} \end{bmatrix}$ , which is the internal model for repetitive control. The details of how to select  $W_u$  can be found in [16] and [18]. A weighting parameter  $\xi_u$  is added to adjust the relative importance of  $v_u$  with respect to  $w_u$ , and another weighting parameter  $\mu_u$  is added to adjust the relative importance of  $u_u$  with respect to  $b_u$ . The parameters  $\xi_u$  and  $\mu_u$  also play a role in guaranteeing the stability of the system; see more details in [16] and [18]. It can be found out that the generalized plant  $\tilde{P}_u$  is realized as

$$\tilde{P}_u = \begin{bmatrix} A_u & 0 & 0 & B_{u1} & B_{u2} \\ B_{w_u}C_{u1} & A_{w_u} & B_{w_u}\xi_u & B_{w_u}D_{u1} & B_{w_u}D_{u2} \\ \hline D_{w_u}C_{u1} & C_{w_u} & D_{w_u}\xi_u & D_{w_u}D_{u1} & D_{w_u}D_{u2} \\ 0 & 0 & 0 & 0 & \mu_u \\ \hline C_{u1} & 0 & \xi_u & D_{u1} & D_{u2} \end{bmatrix} \quad (5)$$

The controller  $C_u$  can then be found according to the generalized plant  $\tilde{P}_u$  using the  $H^\infty$  control theory, e.g., by using the function `hinfsyn` provided in MATLAB.

#### IV. DESIGN OF THE CURRENT CONTROLLER

As explained before, when designing the outer-loop current controller, it can be assumed that the inner voltage loop tracks the reference voltage perfectly, i.e.,  $u_o = u_{\text{ref}}$ . Hence, the control plant for the current loop is simply the grid inductor, as shown in Fig. 3. The formulation of the  $H^\infty$  control problem to design the  $H^\infty$  compensator  $C_i$  is similar to that in the case of the voltage control loop shown in Fig. 5 but with a different plant  $P_i$  and the subscript  $u$  replaced with  $i$ .

##### A. State-Space Model of the Plant $P_i$

Since it can be assumed that  $u_o = u_{\text{ref}}$ , there is  $u_o = u_g + u_i$  or  $u_i = u_o - u_g$  from Figs. 3 and 4, i.e.,  $u_i$  is actually the voltage dropped on the grid inductor. The feedforwarded grid voltage  $u_g$  provides a base local load voltage for the inverter. The same voltage  $u_g$  appears on both sides of the grid interface inductor  $L_g$ , and it does not affect the controller design. Hence, the feedforwarded voltage path can be ignored

 TABLE I  
PARAMETERS OF THE INVERTER

Parameter	Value	Parameter	Value
$L_f$	$150\mu\text{H}$	$R_f$	$0.045\Omega$
$L_g$	$450\mu\text{H}$	$R_g$	$0.135\Omega$
$C_f$	$22\mu\text{F}$	$R_d$	$1\Omega$

during the design process. This is a very important feature. The only contribution that needs to be considered during the design process is the output  $u_i$  of the repetitive current controller.

The grid current  $i_2$  flowing through the grid interface inductor  $L_g$  is chosen as the state variable  $x_i = i_2$ . The external input is  $w_i = i_{\text{ref}}$ , and the control input is  $u_i$ . The output signal from the plant  $P_i$  is the tracking error  $e_i = i_{\text{ref}} - i_2$ , i.e., the difference between the current reference and the grid current. The plant  $P_i$  can then be described by the state equation

$$\dot{x}_i = A_i x_i + B_{i1} w_i + B_{i2} u_i$$

and the output equation

$$y_i = e_i = C_{i1} x_i + D_{i1} w_i + D_{i2} u_i$$

where

$$A_i = -\frac{R_g}{L_g} \quad B_{i1} = 0 \quad B_{i2} = \frac{1}{L_g}$$

$$C_{i1} = -1 \quad D_{i1} = 1 \quad D_{i2} = 0.$$

The corresponding transfer function of  $P_i$  is

$$P_i = \left[ \begin{array}{c|cc} A_i & B_{i1} & B_{i2} \\ \hline C_{i1} & D_{i1} & D_{i2} \end{array} \right].$$

##### B. Formulation of the Standard $H^\infty$ Problem

Similarly, a standard  $H^\infty$  problem can be formulated as in the case of the voltage controller shown in Fig. 5, replacing the subscript  $u$  with  $i$ . The resulting generalized plant can be obtained as

$$\tilde{P}_i = \begin{bmatrix} A_i & 0 & 0 & B_{i1} & B_{i2} \\ B_{w_i}C_{i1} & A_{w_i} & B_{w_i}\xi_i & B_{w_i}D_{i1} & B_{w_i}D_{i2} \\ \hline D_{w_i}C_{i1} & C_{w_i} & D_{w_i}\xi_i & D_{w_i}D_{i1} & D_{w_i}D_{i2} \\ 0 & 0 & 0 & 0 & \mu_i \\ \hline C_{i1} & 0 & \xi_i & D_{i1} & D_{i2} \end{bmatrix} \quad (6)$$

with weighting parameters  $\xi_i$  and  $\mu_i$  and low-pass filter  $W_i = \begin{bmatrix} A_{w_i} & B_{w_i} \\ C_{w_i} & D_{w_i} \end{bmatrix}$ , which can be selected similarly as the corresponding ones for the voltage controller.

The controller  $C_i$  can then be found according to the generalized plant  $\tilde{P}_i$  using the  $H^\infty$  control theory, e.g., by using the function `hinfsyn` provided in MATLAB.

#### V. DESIGN EXAMPLE

As an example, the controllers will be designed in this section for an experimental setup, which consists of an inverter

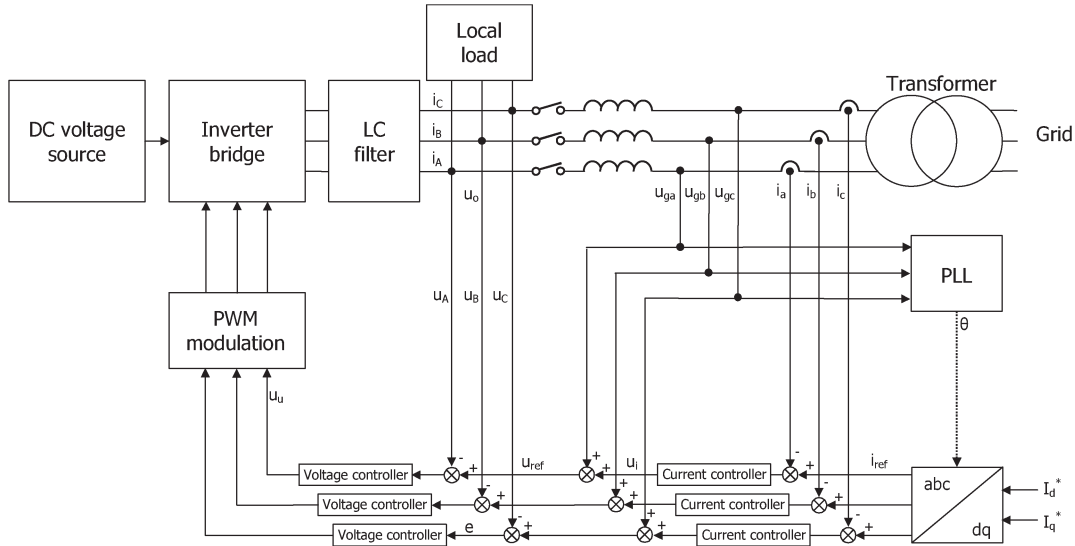


Fig. 6. Sketch of a grid-connected three-phase inverter using the proposed strategy.

board, a three-phase  $LC$  filter, a three-phase grid interface inductor, a board consisting of voltage and current sensors, a step-up wye-wye transformer (12 V/230 V/50 Hz), a dSPACE DS1104 R&D controller board with ControlDesk software, and MATLAB Simulink/SimPower software package. The inverter board consists of two independent three-phase inverters and has the capability to generate PWM voltages from a constant 42-V dc voltage source. One inverter was used to generate a stable neutral line for the three-phase inverter. The generated three-phase voltage was connected to the grid via a controlled circuit breaker and a step-up transformer. The PWM switching frequency was 12 kHz. A Yokogawa power analyzer WT1600 was used to measure the THD. The parameters of the inverter are given in Table I. Three sets of identical controllers were used for the three phases because there was a stable neutral line available. The control structure for the three-phase system is shown in Fig. 6. A traditional  $dq$  PLL was used to provide the phase information needed to generate the three-phase grid current references via a  $dq/abc$  transformation from the current references  $I_d^*$  and  $I_q^*$ . The internal model was implemented according to [16], with the capability to adapt to the frequency change in the grid.

It is worth noting that it is quite a challenge to work with low-voltage inverters to improve the voltage THD, because, in general, the higher the voltage, the bigger the value of the fundamental component. Moreover, the impact of noises and disturbances is more severe for low-voltage systems than for high-voltage ones. Hence, it should be easy to apply the strategy proposed in this paper to inverters at higher voltage and higher power ratings.

#### A. Design of the $H^\infty$ Voltage Controller

According to [16] and [18], the weighting function was chosen as  $W_u = \begin{bmatrix} -2555 & 2550 \\ 1 & 1 \end{bmatrix}$  for  $f = 50$  Hz, and the weighting parameters were chosen as  $\xi_u = 100$  and  $\mu_u = 1.85$ . For the parameters of the plant given in Table I, the  $H^\infty$

controller  $C_u$  which nearly minimizes the  $H^\infty$  norm of the transfer matrix from  $\tilde{w}_u$  to  $\tilde{z}_u$  was obtained by using the MATLAB function *hinfsyn* (which solves the standard  $H^\infty$  control problem) as

$$C_u(s) = \frac{748.649(s^2 + 6954s + 3.026 \times 10^8)}{(s + 2550)(s^2 + 7969s + 3.043 \times 10^8)}.$$

It can be reduced to

$$C_u(s) = \frac{748.649}{s + 2550}$$

without causing noticeable performance degradation, after canceling the poles and zeros that are close to each other.

#### B. Design of the $H^\infty$ Current Controller

According to [16] and [18], the filter  $W_i$  was chosen as  $W_i = \begin{bmatrix} -2555 & 2550 \\ 1 & 1 \end{bmatrix}$ , and the weighting parameters were chosen as  $\xi_i = 100$  and  $\mu_i = 1.8$ . The  $H^\infty$  controller  $C_i$  which nearly minimizes the  $H^\infty$  norm of the transfer matrix from  $\tilde{w}_i$  to  $\tilde{z}_i$  was obtained by using the MATLAB function *hinfsyn* as

$$C_i(s) = \frac{177980833.6502(s + 300)}{(s + 4.334 \times 10^8)(s + 2550)}.$$

The factor  $s + 4.334 \times 10^8$  in the denominator can be approximated with the constant  $4.334 \times 10^8$  without causing any noticeable performance change. The resulting reduced controller is

$$C_i(s) = \frac{0.4107(s + 300)}{s + 2550}.$$

## VI. EXPERIMENTAL RESULTS

The above-designed controller was implemented to evaluate its performance in both stand-alone and grid-connected modes with different loads. The seamless transfer of the operation

modes was also carried out. The  $H^\infty$  repetitive current controller was replaced with a proportional-resonant (PR) current controller for comparison in the grid-connected mode. In the stand-alone mode, since the grid current reference was set to zero and the circuit breaker was turned off (which means that the current controller was not functioning), the experimental results with both the repetitive current controller and the PR current controller are similar, and hence, no comparative results are provided for the stand-alone mode. The PR controller was designed according to [31] with the plant used in Section IV-A as

$$C_{i-PR}(s) = 0.735 + \frac{20s}{s^2 + 10000\pi^2}$$

A. In the Stand-Alone Mode

The voltage reference was set to the grid voltage (the inverter is synchronized and ready to be connected to the utility grid). The evaluation of the proposed controller was made for a resistive load ( $R_A = R_B = R_C = 12 \Omega$ ), a nonlinear load (a three-phase uncontrolled rectifier loaded with an LC filter with  $L = 150 \mu\text{H}$  and  $C = 1000 \mu\text{F}$  and a resistor  $R = 20 \Omega$ ), and an unbalanced load ( $R_A = R_C = 12 \Omega$  and  $R_B = \infty$ ).

1) *With the Resistive Load:* The local load voltage  $u_A$ , voltage reference  $u_{ref}$ , and filter inductor current  $i_A$  are shown in Fig. 7(a). Fig. 7(b) shows the spectra of the inverter local load voltage and the local load current. The recorded local voltage THD was 1.27%, while the grid voltage THD was 1.8%. Since the utility grid voltage was used as the reference, it is worth mentioning that the quality of the inverter local load voltage was better than that of the grid voltage, even without using an active filter.

2) *With the Nonlinear Load:* The local load voltage  $u_A$ , voltage reference  $u_{ref}$ , and filter inductor current  $i_A$  are shown in Fig. 8(a). The spectra of the inverter local load voltage and the local load current are shown in Fig. 8(b). The recorded local load voltage THD was 4.73%, while the grid voltage THD was 1.78%. The experimental results demonstrate satisfactory performance of the voltage controller for nonlinear loads.

3) *With the Unbalanced Load:* The inverter local load voltage and the local load currents are shown in Fig. 9(a) with their spectra shown in Fig. 9(b). The recorded local load voltage THD was 1.27%, while the grid voltage THD was 1.77%. Since the proposed control structure adopts separate controllers for each phase, the unbalanced loads had no influence on the voltage controller performance, and the inverter local load voltages remained balanced.

B. In the Grid-Connected Mode

The current reference of the grid current  $I_d^*$  was set at 2 A (corresponding to 1.41 A rms), after connecting the inverter to the grid. The reactive power was set at 0 var ( $I_q^* = 0$ ). The resistive, nonlinear, and unbalanced loads used in the previous section were used again. Moreover, the case without a local load was carried out as well. Finally, the transient responses of the system were evaluated.

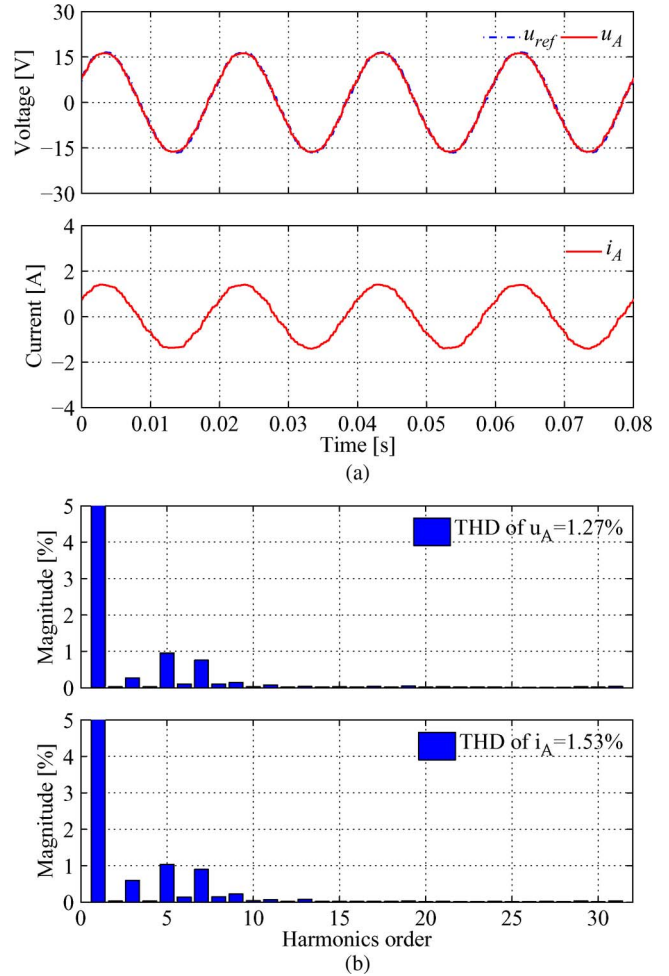


Fig. 7. Stand-alone mode with a resistive load. (a) (Upper)  $u_A$  and its reference  $u_{ref}$  and (lower) current  $i_A$ . (b) (Upper) Voltage THD and (lower) current THD.

1) *Without a Local Load:* The local load voltage  $u_A$ , the voltage tracking error  $e_u$ , the grid current  $i_a$ , and the current tracking error  $e_i$  are shown in the left column of Fig. 10(a) for the case with the  $H^\infty$  current controller and in the left column of Fig. 10(b) for the case with the PR current controller. The spectra of the inverter local load voltage and the grid current of both controllers are shown in the left column of Fig. 11. The recorded THD of the local voltage was 0.99% for the proposed controller and 0.99% for the PR controller, while the grid voltage THDs were 1.58% and 0.96%, respectively. The THD of the grid current was 2.27% for the proposed  $H^\infty$  controller and 5.09% for the PR controller. In this experiment, the proposed controller outperforms the PR-current- $H^\infty$ -voltage controller. Note that the grid was cleaner when the PR-current- $H^\infty$ -voltage controller was tested.

2) *With the Resistive Load:* The experimental results of the grid-connected inverter with the balanced resistive local load connected to the system are shown in the middle column of Fig. 10. The spectra of the inverter local load voltages and grid currents are shown in the middle-left column of Fig. 11. When the resistive local load is connected, the recorded local load voltage THD was 1.21% for the proposed  $H^\infty$  controller and 0.97% for the PR controller, while the grid voltage THDs

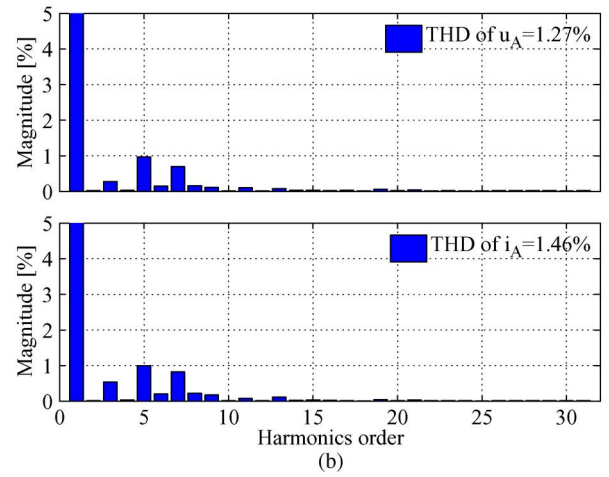
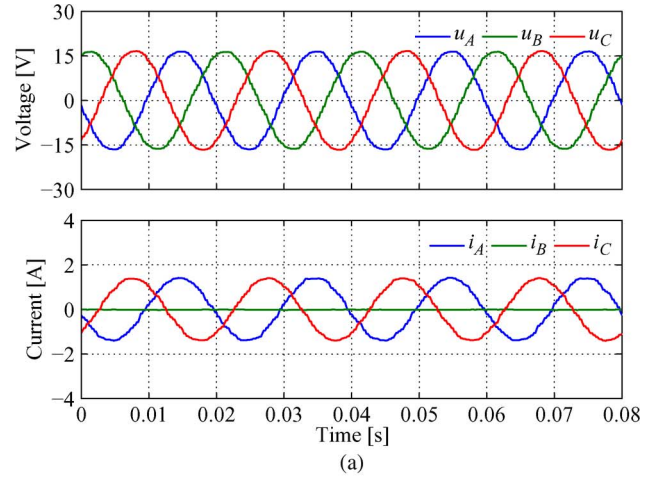
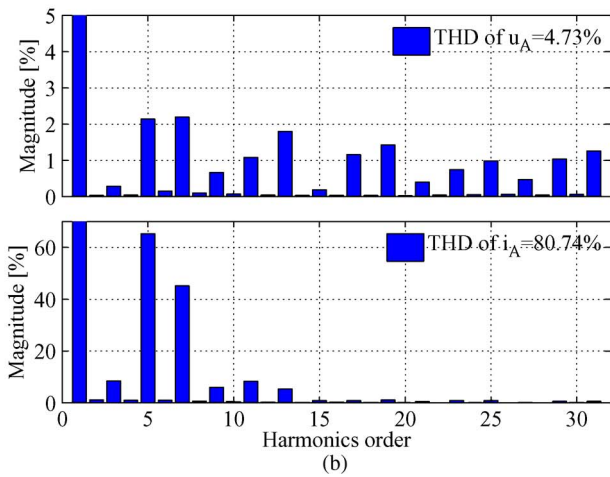
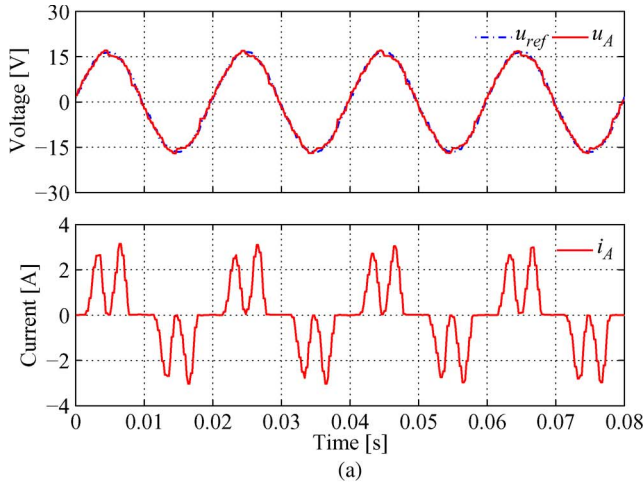


Fig. 8. Stand-alone mode with a nonlinear load. (a) (Upper)  $u_A$  and its reference  $u_{ref}$  and (lower) current  $i_A$ . (b) (Upper) Voltage THD and (lower) current THD.

Fig. 9. Stand-alone mode with an unbalanced load. (a) (Upper) Inverter local load voltage and (lower) local load currents. (b) (Upper) Voltage THD and (lower) current THD.

were 1.8% and 0.95%, respectively. The grid current THD was 2.32% for the proposed  $H^\infty$  controller and 5.24% for the PR controller. The performance of both controllers remains almost unchanged with comparison to the previous experiment without a local load. The proposed controller again outperforms the PR-current- $H^\infty$ -voltage controller. Note that the grid was cleaner again when the PR-current- $H^\infty$ -voltage controller was tested.

3) *With the Nonlinear Load:* The local load voltage  $u_A$ , the voltage tracking error  $e_u$ , the grid current  $i_a$ , and the current tracking error  $e_i$  are shown in the right column of Fig. 10(a) for the case with the  $H^\infty$  current controller and in the right column of Fig. 10(b) for the case with the PR current controller. The spectra of the inverter local load voltage and the grid current are shown in the middle-right column of Fig. 11. The recorded THD of the local voltage was 2.22% for the proposed  $H^\infty$  controller and 2.97% for the PR controller, while the grid voltage THDs were 1.72% and 0.93%, respectively. The THDs of the grid current were 5.35% and 7.97%, respectively. The proposed controller again clearly outperforms the PR-current- $H^\infty$ -voltage controller.

4) *With the Unbalanced Load:* The inverter local load voltage, the filter inductor current, and the grid current are shown in Fig. 12(a) for the case with the  $H^\infty$  current controller and in 12(b) for the case with the PR current controller. The spectra

of the inverter local load voltage and the grid current are shown in the right column of Fig. 11. The recorded local load voltage THD was 1.09% in the case with the  $H^\infty$  current controller and 1.00% in the case with the PR controller, while the grid voltage THDs were 1.77% and 0.92%, respectively. The grid current THDs were 2.36% and 5.20%, respectively. Both strategies can inject balanced clean currents to the grid although the local load is not balanced.

### C. Transient Performance

1) *Transient Response to the Change of the Grid Current Reference (No Local Load Connected):* A step change in the grid current  $I_d^*$  reference from 2 A (1.41 A rms) to 3 A (2.12 A rms) was applied (while keeping  $I_q^* = 0$ ). The grid current  $i_a$ , its reference  $i_{ref}$ , and the current tracking error  $e_i$  are shown in Fig. 13. The proposed controller took about 12 cycles to settle down, and the PR-current- $H^\infty$ -voltage controller took about eight cycles to settle down. This is reasonable because each repetitive controller takes about five cycles to settle down. This reflects the tradeoff between low THD and system response speed.

2) *Transient Response to the Change of the Resistive Local Load:* The filter inductor current and the grid current, together

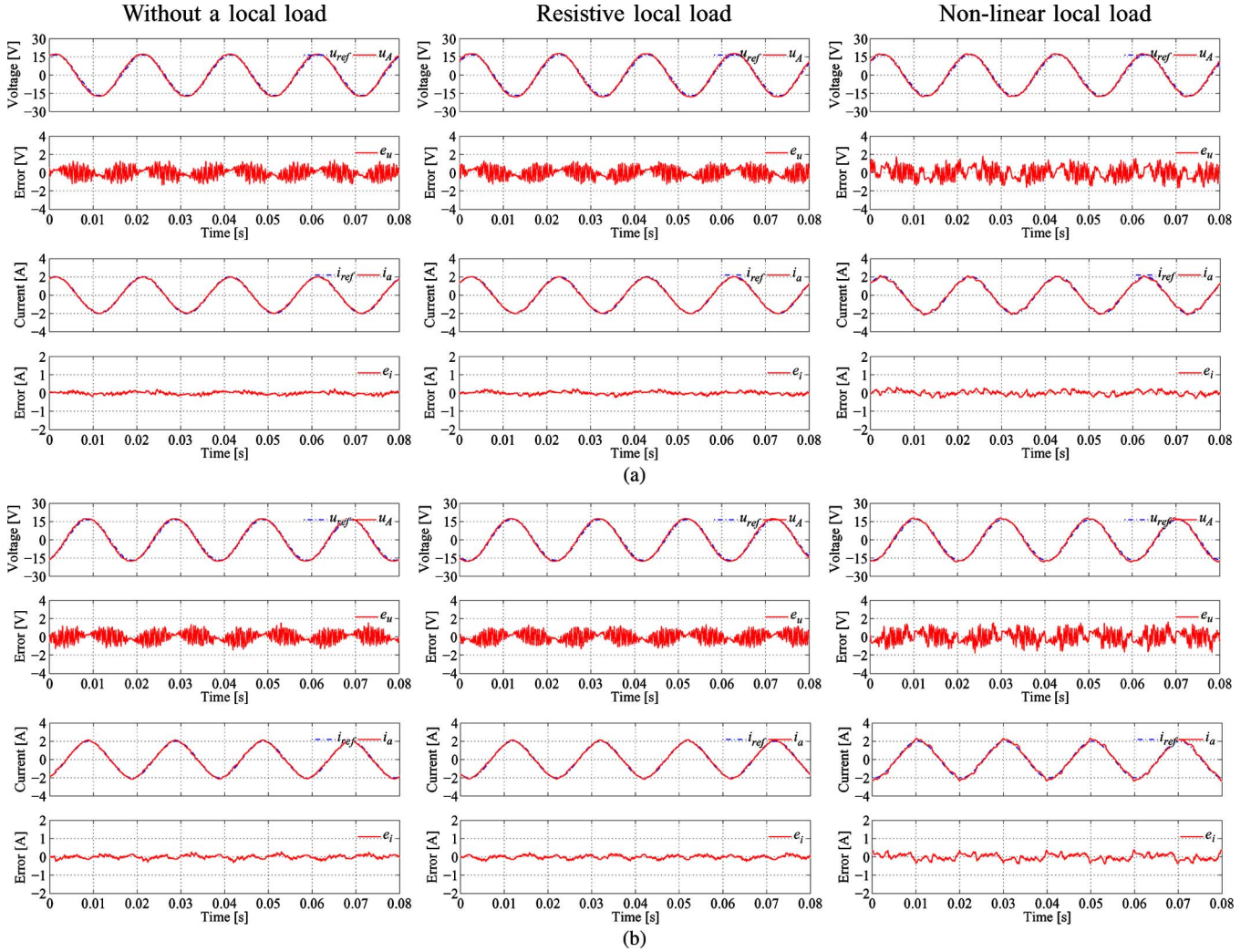


Fig. 10. Inverter local load voltage and the grid current in the grid-connected mode with (left column) no load, (middle column) resistive load, and (right column) nonlinear load. (a)  $H^\infty$  repetitive current-voltage controller. (b) PR-current- $H^\infty$ -repetitive-voltage controller.

with the reference current and the tracking error, when the three-phase resistive local load was changed from  $R_A = R_B = R_C = 12 \Omega$  to  $R_A = R_B = R_C = 100 \Omega$  and back, are shown in Fig. 14. The detailed grid current and the reference current, together with the current tracking error, and the inverter local load voltage and its reference, together with the tracking error, during the changes are shown in Fig. 15 for the change from 12 to 100  $\Omega$  at  $t = 1.88$  s and in Fig. 16 for the change from 100 to 12  $\Omega$  at  $t = 6.61$  s. The current controller took about five cycles to settle down, which is in line with the findings from the previous experiment. There was no noticeable change in the inverter local load voltage.

#### D. Seamless Transfer of the Operation Mode

The transient response of the grid current when the inverter was changed from the stand-alone mode to the grid-connected mode and back is shown in Fig. 17. The detailed responses during the transfers are shown in Figs. 18–20.

At  $t = 1$  s, the inverter was connected to the grid. The details of the transfer from the stand-alone mode to the grid-connected mode are shown in Fig. 18. There was not much dynamics

in the current. There was no noticeable change in the inverter local load voltage either. Hence, seamless grid connection was achieved.

A step change in the grid current reference  $I_d^*$  from 0 to 1.5 A (1.06 A rms) was applied at time  $t = 3$  s, and the responses are shown in Fig. 19(a) and (b). The system took about 12 cycles to settle down, which is consistent with the test done in Section VI-C1.

At  $t = 7.08$  s, the inverter was disconnected from the grid, and the details of the responses are shown in Fig. 20(a) and (b). There was no noticeable transients in the inverter local load voltage, and seamless disconnection from the grid was achieved.

In summary, the proposed control strategy is able to achieve seamless transfer of operation modes from stand-alone to grid-connected or *vice versa*.

## VII. CONCLUSION

The cascaded current-voltage control strategy has been proposed for inverters in microgrids. It consists of an inner voltage loop and an outer current loop and offers excellent performance



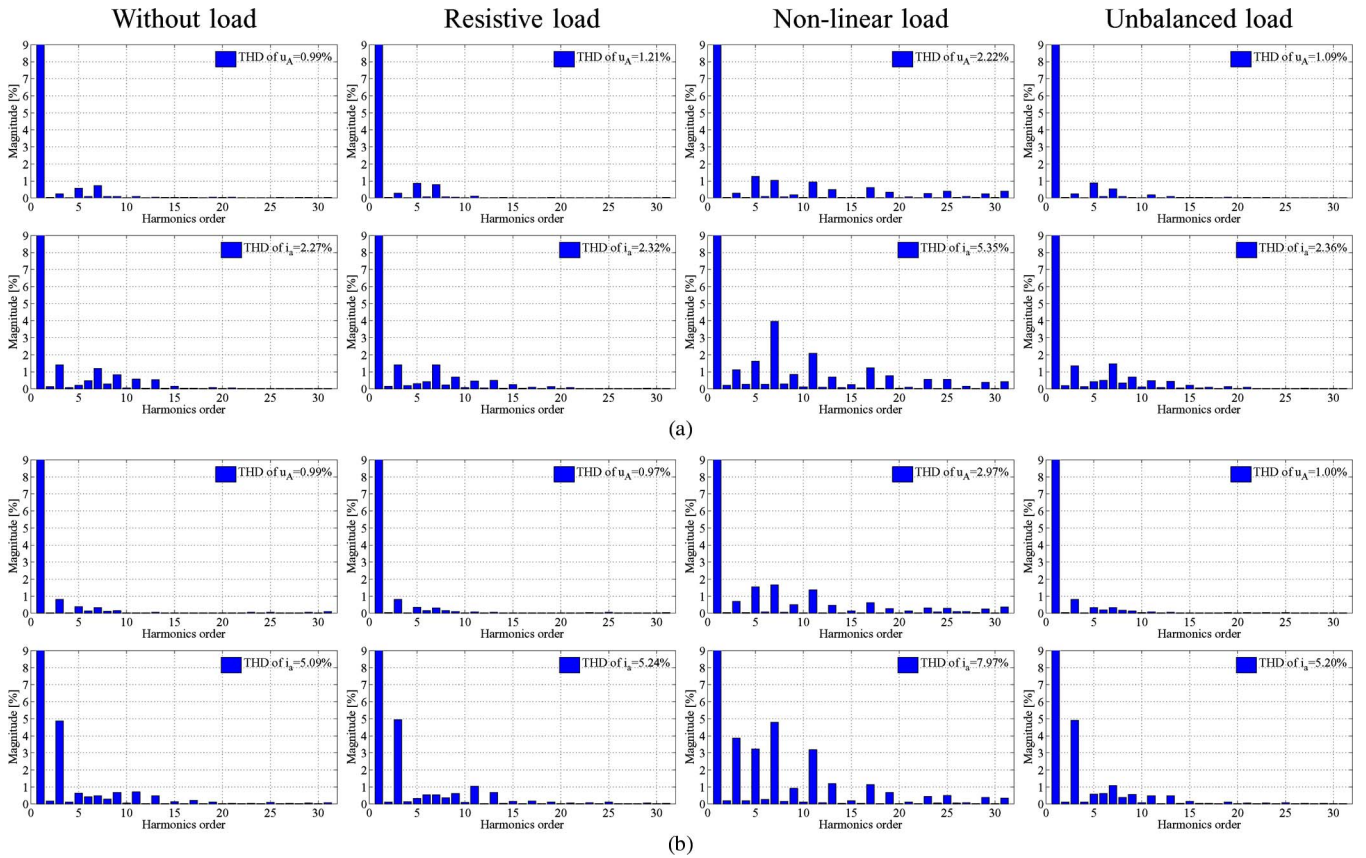


Fig. 11. Spectra of the inverter local load voltage and the grid current with (left column) no load, resistive load (middle-left column), (middle-right column) nonlinear load, and (right column) unbalanced load. (a)  $H^\infty$  repetitive current-voltage controller. (b) PR-current- $H^\infty$ -repetitive-voltage controller.

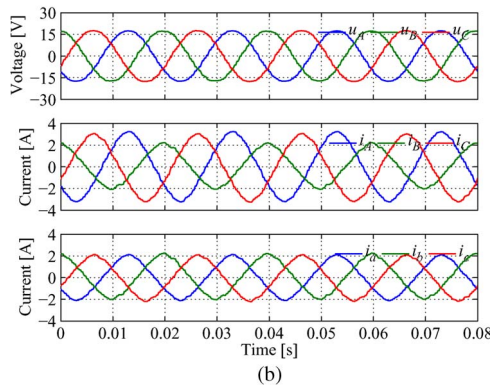
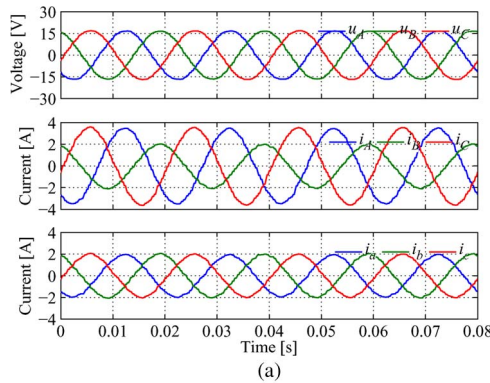


Fig. 12. Grid-connected mode with unbalanced loads: (Upper) Inverter local load voltage, (middle) the filter inductor currents, and (lower) the grid currents. (a)  $H^\infty$  repetitive current-voltage controller. (b) PR-current- $H^\infty$ -repetitive-voltage controller.

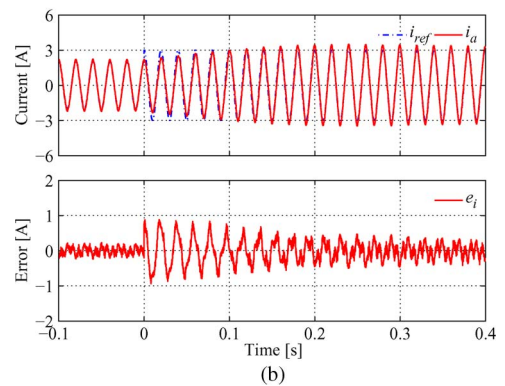
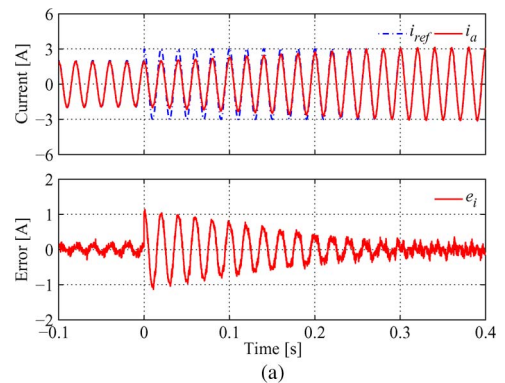


Fig. 13. Transient response in the grid-connected mode without local load to 1-A step change in  $I_d^*$ : (Upper) Grid current  $i_a$  and its reference  $i_{ref}$  and (lower) current tracking error  $e_i$ . (a)  $H^\infty$  repetitive current-voltage controller. (b) PR-current- $H^\infty$ -repetitive-voltage controller.

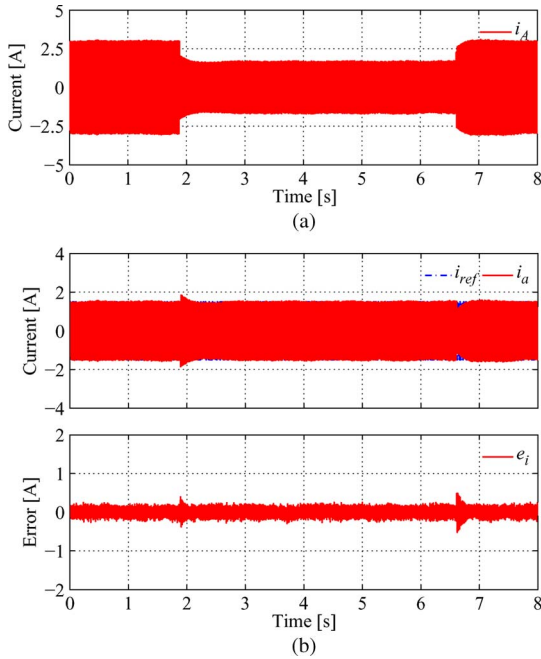


Fig. 14. Transient responses of the inverter and grid currents when the local load was changed. (a) Filter inductor current  $i_A$ . (b) Grid current  $i_a$ , its reference  $i_{ref}$ , and the current tracking error  $e_i$ .

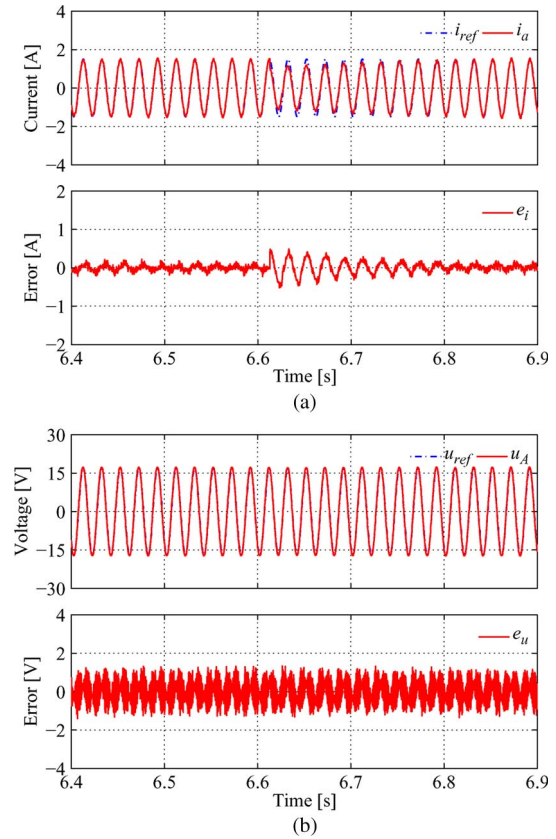


Fig. 16. Details of the responses when the local load was changed back from 100 to 12  $\Omega$  at  $t = 6.61$  s. (a)  $i_a$ , its reference  $i_{ref}$ , and the current tracking error  $e_i$ . (b)  $u_A$ , its reference  $u_{ref}$ , and the voltage tracking error  $e_u$ .

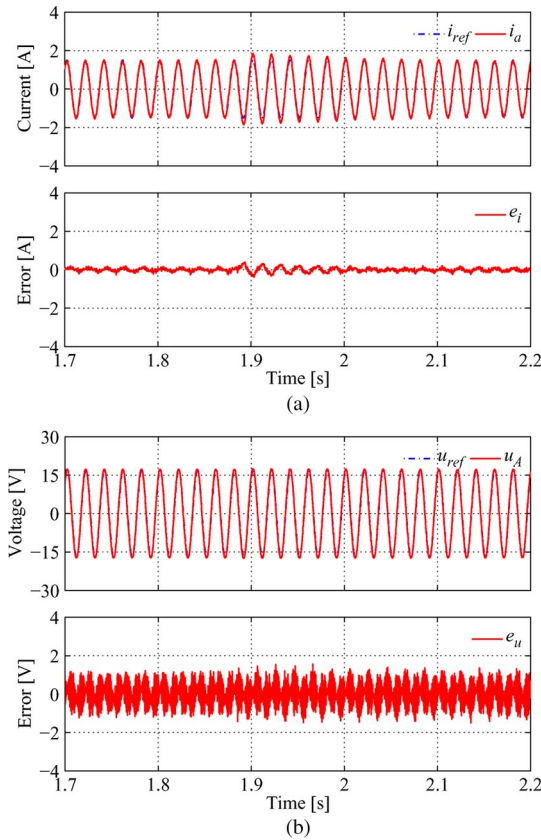


Fig. 15. Details of the responses when the local load was changed from 12 to 100  $\Omega$  at  $t = 1.88$  s. (a)  $i_a$ , its reference  $i_{ref}$ , and the current tracking error  $e_i$ . (b)  $u_A$ , its reference  $u_{ref}$ , and the voltage tracking error  $e_u$ .

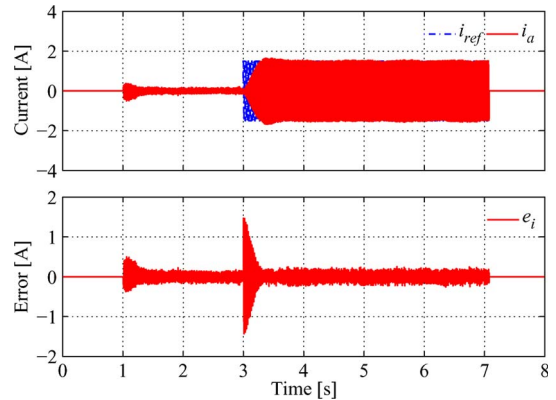


Fig. 17. Transient response of the inverter when transferred from the stand-alone mode to the grid-connected mode and then back.

in terms of THD for both the inverter local load voltage and the grid current. In particular, when nonlinear and/or unbalanced loads are connected to the inverter in the grid-connected mode,

the proposed strategy significantly improves the THD of the inverter local load voltage and the grid current at the same time. The controllers are designed using the  $H^\infty$  repetitive control in this paper but can be designed using other approaches as well. The proposed strategy also achieves seamless transfer between the stand-alone and the grid-connected modes. The strategy can be used for single-phase systems or three-phase systems. As a result, the nonlinear harmonic currents and unbalanced local load currents are all contained locally and do not affect the grid. Experimental results under various scenarios have demonstrated the excellent performance of the proposed strategy.

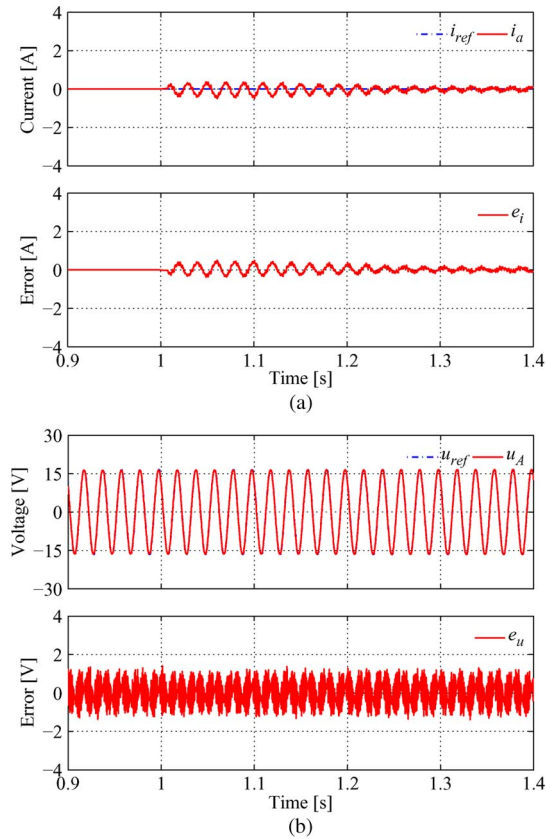


Fig. 18. Details of the responses when transferred from the stand-alone mode to the grid-connected mode at  $t = 1$  s. (a)  $i_a$ , its reference  $i_{ref}$ , and the current tracking error  $e_i$ . (b)  $u_A$ , its reference  $u_{ref}$ , and the voltage tracking error  $e_u$ .

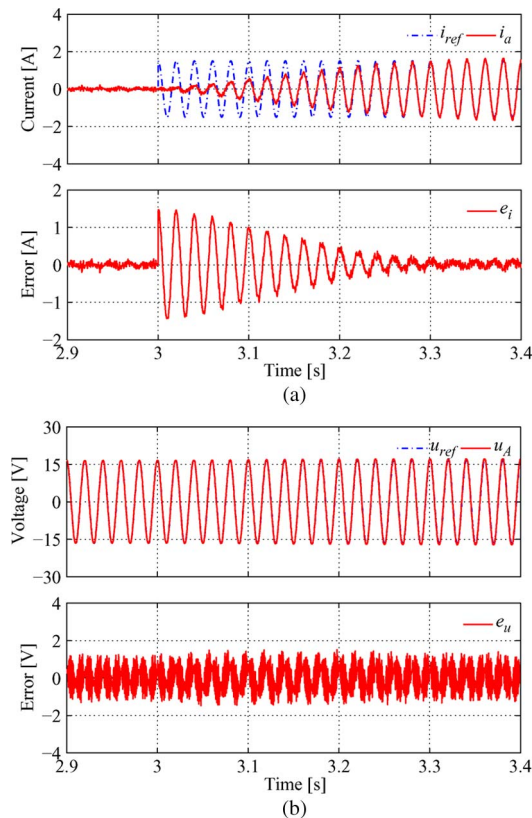


Fig. 19. Details of the responses to a step change in the grid current reference  $I_d^*$  from 0 to 1.5 A at  $t = 3$  s. (a)  $i_a$ , its reference  $i_{ref}$ , and the current tracking error  $e_i$ . (b)  $u_A$ , its reference  $u_{ref}$ , and the voltage tracking error  $e_u$ .

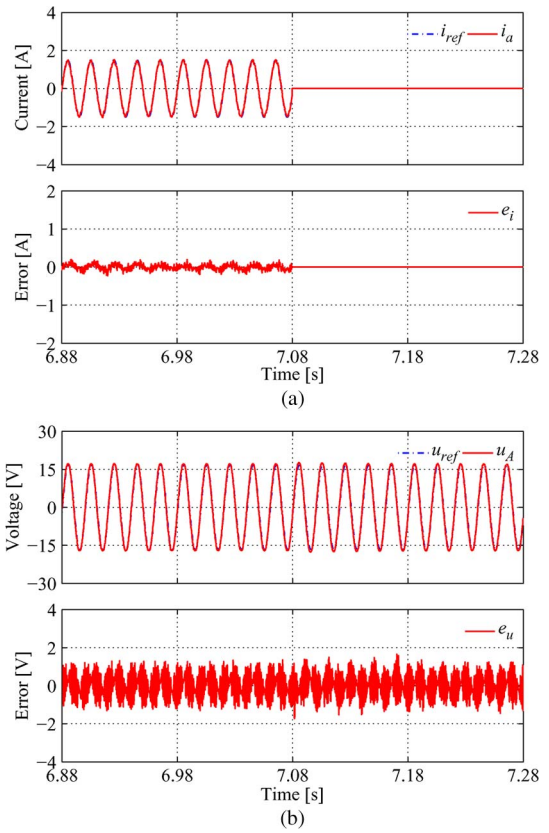


Fig. 20. Details of the responses when transferred from the grid-connected mode to the stand-alone mode at  $t = 7.08$  s. (a)  $i_a$ , its reference  $i_{ref}$ , and the current tracking error  $e_i$ . (b)  $u_A$ , its reference  $u_{ref}$ , and the voltage tracking error  $e_u$ .

#### ACKNOWLEDGMENT

The authors would like to thank the reviewers and editors for their detailed comments, which have considerably improved the quality of this paper. Author Q.-C. Zhong would also like to thank Yokogawa Measurement Technologies, Ltd., for the donation of a high-precision wide-bandwidth power meter WT1600.

#### REFERENCES

- [1] N. Hatziargyriou, H. Asano, R. Irvani, and C. Marnay, "Microgrids," *IEEE Power Energy Mag.*, vol. 5, no. 4, pp. 78–94, Jul./Aug. 2007.
- [2] F. Katiraei, R. Irvani, N. Hatziargyriou, and A. Dimeas, "Microgrids management," *IEEE Power Energy Mag.*, vol. 6, no. 3, pp. 54–65, May/Jun. 2008.
- [3] C. Xiarnay, H. Asano, S. Papathanassiou, and G. Strbac, "Policymaking for microgrids," *IEEE Power Energy Mag.*, vol. 6, no. 3, pp. 66–77, May/Jun. 2008.
- [4] Y. Mohamed and E. El-Saadany, "Adaptive decentralized droop controller to preserve power sharing stability of paralleled inverters in distributed generation microgrids," *IEEE Trans. Power Electron.*, vol. 23, no. 6, pp. 2806–2816, Nov. 2008.
- [5] Y. Li and C.-N. Kao, "An accurate power control strategy for power-electronics-interfaced distributed generation units operating in a low-voltage multibus microgrid," *IEEE Trans. Power Electron.*, vol. 24, no. 12, pp. 2977–2988, Dec. 2009.
- [6] C.-L. Chen, Y. Wang, J.-S. Lai, Y.-S. Lee, and D. Martin, "Design of parallel inverters for smooth mode transfer microgrid applications," *IEEE Trans. Power Electron.*, vol. 25, no. 1, pp. 6–15, Jan. 2010.
- [7] J. Guerrero, J. Vasquez, J. Matas, M. Castilla, and L. de Vicuna, "Control strategy for flexible microgrid based on parallel line-interactive UPS systems," *IEEE Trans. Ind. Electron.*, vol. 56, no. 3, pp. 726–736, Mar. 2009.

- [8] Z. Yao, L. Xiao, and Y. Yan, "Seamless transfer of single-phase grid-interactive inverters between grid-connected and stand-alone modes," *IEEE Trans. Power Electron.*, vol. 25, no. 6, pp. 1597–1603, Jun. 2010.
- [9] Q.-C. Zhong and G. Weiss, "Synchronverters: Inverters that mimic synchronous generators," *IEEE Trans. Ind. Electron.*, vol. 58, no. 4, pp. 1259–1267, Apr. 2011.
- [10] Q.-C. Zhong, "Robust droop controller for accurate proportional load sharing among inverters operated in parallel," *IEEE Trans. Ind. Electron.*, vol. 60, no. 4, pp. 1281–1290, Apr. 2013.
- [11] M. Prodanovic and T. Green, "High-quality power generation through distributed control of a power park microgrid," *IEEE Trans. Ind. Electron.*, vol. 53, no. 5, pp. 1471–1482, Oct. 2006.
- [12] Y. W. Li, D. Vilathgamuwa, and P. C. Loh, "A grid-interfacing power quality compensator for three-phase three-wire microgrid applications," *IEEE Trans. Power Electron.*, vol. 21, no. 4, pp. 1021–1031, Jul. 2006.
- [13] D. Vilathgamuwa, P. C. Loh, and Y. Li, "Protection of microgrids during utility voltage sags," *IEEE Trans. Ind. Electron.*, vol. 53, no. 5, pp. 1427–1436, Oct. 2006.
- [14] F. Blaabjerg, R. Teodorescu, M. Liserre, and A. Timbus, "Overview of control and grid synchronization for distributed power generation systems," *IEEE Trans. Ind. Electron.*, vol. 53, no. 5, pp. 1398–1409, Oct. 2006.
- [15] G. Weiss, Q.-C. Zhong, T. Green, and J. Liang, " $H^\infty$  repetitive control of DC-AC converters in micro-grids," *IEEE Trans. Power Electron.*, vol. 19, no. 1, pp. 219–230, Jan. 2004.
- [16] T. Hornik and Q.-C. Zhong, " $H^\infty$  repetitive voltage control of grid-connected inverters with frequency adaptive mechanism," *IET Proc. Power Electron.*, vol. 3, no. 6, pp. 925–935, Nov. 2010.
- [17] T. Hornik and Q.-C. Zhong, " $H^\infty$  repetitive current controller for grid-connected inverters," in *Proc. 35th IEEE IECON*, 2009, pp. 554–559.
- [18] T. Hornik and Q.-C. Zhong, "A current control strategy for voltage-source inverters in microgrids based on  $H^\infty$  and repetitive control," *IEEE Trans. Power Electron.*, vol. 26, no. 3, pp. 943–952, Mar. 2011.
- [19] Q.-C. Zhong, J. Liang, G. Weiss, C. Feng, and T. Green, " $H^\infty$  control of the neutral point in 4-wire 3-phase DC-AC converters," *IEEE Trans. Ind. Electron.*, vol. 53, no. 5, pp. 1594–1602, Nov. 2006.
- [20] S. Hara, Y. Yamamoto, T. Omata, and M. Nakano, "Repetitive control system: A new type servo system for periodic exogenous signals," *IEEE Trans. Autom. Control*, vol. 33, no. 7, pp. 659–668, Jul. 1988.
- [21] B. Francis and W. Wonham, "The internal model principle for linear multivariable regulators," *Applied Mathematics and Optimization*, vol. 2, no. 2, pp. 170–194, Jun. 1975.
- [22] Y. Ye, B. Zhang, K. Zhou, D. Wang, and Y. Wang, "High-performance repetitive control of PWM DC-AC converters with real-time phase lead FIR filter," *IEEE Trans. Circuits Syst. II, Exp. Briefs*, vol. 53, no. 8, pp. 768–772, Aug. 2006.
- [23] B. Zhang, D. Wang, K. Zhou, and Y. Wang, "Linear phase lead compensation repetitive control of a CVCF PWM inverter," *IEEE Trans. Ind. Electron.*, vol. 55, no. 4, pp. 1595–1602, Apr. 2008.
- [24] S. Chen, Y. Lai, S.-C. Tan, and C. Tse, "Analysis and design of repetitive controller for harmonic elimination in PWM voltage source inverter systems," *IET Proc. Power Electron.*, vol. 1, no. 4, pp. 497–506, Dec. 2008.
- [25] Y.-Y. Tzou, S.-L. Jung, and H.-C. Yeh, "Adaptive repetitive control of PWM inverters for very low THD AC-voltage regulation with unknown loads," *IEEE Trans. Power Electron.*, vol. 14, no. 5, pp. 973–981, Sep. 1999.
- [26] K. Zhou, D. Wang, B. Zhang, and Y. Wang, "Plug-in dual-mode-structure repetitive controller for CVCF PWM inverters," *IEEE Trans. Ind. Electron.*, vol. 56, no. 3, pp. 784–791, Mar. 2009.
- [27] R. Mastromauro, M. Liserre, T. Kerekes, and A. Dell'Aquila, "A single-phase voltage-controlled grid-connected photovoltaic system with power quality conditioner functionality," *IEEE Trans. Ind. Electron.*, vol. 56, no. 11, pp. 4436–4444, Nov. 2009.
- [28] A. Garcia-Cerrada, O. Pinzon-Ardila, V. Feliu-Battle, P. Roncero-Sanchez, and P. Garcia-Gonzalez, "Application of a repetitive controller for a three-phase active power filter," *IEEE Trans. Power Electron.*, vol. 22, no. 1, pp. 237–246, Jan. 2007.
- [29] G. Escobar, P. Hernandez-Briones, P. Martinez, M. Hernandez-Gomez, and R. Torres-Olguin, "A repetitive-based controller for the compensation of harmonic components," *IEEE Trans. Ind. Electron.*, vol. 55, no. 8, pp. 3150–3158, Aug. 2008.
- [30] P. C. Loh and D. Holmes, "Analysis of multiloop control strategies for LC/CL/LCL-filtered voltage-source and current-source inverters," *IEEE Trans. Ind. Appl.*, vol. 41, no. 2, pp. 644–654, Mar./Apr. 2005.
- [31] A. Timbus, M. Liserre, R. Teodorescu, P. Rodriguez, and F. Blaabjerg, "Evaluation of current controllers for distributed power generation systems," *IEEE Trans. Power Electron.*, vol. 24, no. 3, pp. 654–664, Mar. 2009.



**Qing-Chang Zhong** (M'04–SM'04) received the Diploma in electrical engineering from Hunan Institute of Engineering, Xiangtan, China, in 1990, the M.Sc. degree in electrical engineering from Hunan University, Changsha, China, in 1997, the Ph.D. degree in control theory and engineering from Shanghai Jiao Tong University, Shanghai, China, in 1999, and the Ph.D. degree in control and power engineering from Imperial College London, London, U.K., in 2004.

He was with Technion-Israel Institute of Technology, Haifa, Israel; Imperial College London, London, U.K.; University of Glamorgan, Cardiff, U.K.; University of Liverpool, Liverpool, U.K.; and Loughborough University, Leicestershire, U.K. He currently holds the Chair in control and systems engineering with the Department of Automatic Control and Systems Engineering, The University of Sheffield, Sheffield, U.K. He is the author or coauthor of *Robust Control of Time-Delay Systems* (Springer Verlag, 2006), *Control of Integral Processes With Dead Time* (Springer Verlag, 2010), *Control of Power Inverters in Renewable Energy and Smart Grid Integration* (Wiley-IEEE Press, 2012). His current research focuses on power electronics, electric drives and electric vehicles, distributed generation and renewable energy, smart grid integration, robust and  $H$ -infinity control, time-delay systems, and process control.

Dr. Zhong is a Fellow of the Institution of Engineering and Technology and was a Senior Research Fellow of the Royal Academy of Engineering/Leverhulme Trust, U.K. (2009–2010). He serves as an Associate Editor for the IEEE TRANSACTIONS ON POWER ELECTRONICS and the Conference Editorial Board of the IEEE Control Systems Society. He was a recipient of the Best Doctoral Thesis Prize during his Ph.D. degree at Imperial College London.



**Tomas Hornik** (M'11) received the Diploma in electrical engineering from Technical College V Uzlabine, Prague, Czech Republic, in 1991 and the B.Eng. and Ph.D. degrees in electrical engineering and electronics from the University of Liverpool, Liverpool, U.K., in 2007 and 2010, respectively.

He was a Postdoctoral Researcher with the University of Liverpool from 2010 to 2011. Since 2011, he has been with Turbo Power Systems as a Control Engineer in 2011. His research interests cover power electronics, advanced control theory, and DSP-based control applications. He had more than ten years working experience in industry as a System Engineer responsible for commissioning and software design in power generation and distribution, control systems for central heating systems and building management systems.

Dr. Hornik is a member of the Institution of Engineering and Technology.